Author/s:
Karunaratne, S;Wu, M;Yu, X;Kent, SJ;Silvers, J;Bedggood, P;Metha, A;Mueller, SN;Selva, KJ;Chung, AW;Chinnery, HR;Nguyen, BN;Downie, LE

Title:
Altered Corneal T-Cell Motility and Sensory Nerve Features in Older Adults With Human Immunodeficiency Virus Infection

Date:
2025-09-10

Citation:
Karunaratne, S., Wu, M., Yu, X., Kent, S. J., Silvers, J., Bedggood, P., Metha, A., Mueller, S. N., Selva, K. J., Chung, A. W., Chinnery, H. R., Nguyen, B. N. & Downie, L. E. (2025). Altered Corneal T-Cell Motility and Sensory Nerve Features in Older Adults With Human Immunodeficiency Virus Infection. Investigative Ophthalmology and Visual Science, 66 (12), https://doi.org/10.1167/iovs.66.12.23.

Persistent Link:
https://hdl.handle.net/11343/359710

Altered Corneal T-Cell Motility and Sensory Nerve Features in Older Adults With Human Immunodeficiency Virus Infection

Senuri Karunaratne,[1] Mengliang Wu,[1,2] Xinru Yu,[1] Stephen J. Kent,[2,3] Julie Silvers,[3,†] Phillip Bedggood,[1] Andrew Metha,[1] Scott N. Mueller,[2] Kevin J. Selva,[2] Amy W. Chung,[2] Holly R. Chinnery,[1,4,5] Bao N. Nguyen,[1] and Laura E. Downie[1]

[1]Department of Optometry and Vision Sciences, The University of Melbourne, Melbourne, Australia
[2]Department of Microbiology and Immunology, The Peter Doherty Institute for Infection and Immunity, The University of Melbourne, Melbourne, Australia
[3]Melbourne Sexual Health Centre, Department of Infectious Diseases, Alfred Health, Melbourne, Australia
[4]Department of Optometry and Vision Science, The University of Western Australia, Perth, Australia
[5]Lions Eye Institute, Perth, Australia

Correspondence: Laura E. Downie, Department of Optometry and Vision Sciences, The University of Melbourne, Parkville, Victoria 3010, Australia; ldownie@unimelb.edu.au.

SK and MW contributed equally to this work as joint first authors. BNN and LED contributed equally to this work as joint senior authors.

†Deceased March 17, 2023.

Received: March 15, 2025
Accepted: July 14, 2025
Published: September 10, 2025

Citation: Karunaratne S, Wu M, Yu X, et al. Altered corneal T-cell motility and sensory nerve features in older adults with human immunodeficiency virus infection. *Invest Ophthalmol Vis Sci.* 2025;66(12):23. https://doi.org/10.1167/iovs.66.12.23

Purpose. To characterize corneal immune cell morphodynamics and nerve features, and define the in vivo immune landscape in older adults with human immunodeficiency virus (HIV) receiving antiretroviral therapy (ART), relative to healthy age-matched adults.

Methods. In this cross-sectional study, 16 HIV-positive individuals receiving ART and 15 age-matched controls underwent ocular surface examinations and functional in vivo confocal microscopy (Fun-IVCM). Time-lapsed videos were created to analyze corneal immune cells (T cells, dendritic cells [DCs], macrophages). Subclinical indicators of corneal health (sensory nerve and endothelial cell features), clinical ocular surface findings, and tear cytokines (analyzed using multiplex bead-based immunoassay) were compared between groups.

Results. Participants comprised mostly males (HIV 71 ± 5 years; male:female 15:1; controls 67 ± 6 years; 14:1). The HIV-positive group showed less T-cell motility at the corneal whorl relative to the control group ($P = 0.01$), and region-dependent differences in T-cell speed ($P = 0.001$) and DC area ($P < 0.001$). The HIV-positive group showed greater central corneal nerve fiber width ($P = 0.004$) and larger endothelial cells ($P = 0.02$). Clinical findings, corneal immune cell densities, and tear cytokine profiles were similar between groups.

Conclusions. Among older individuals with well-controlled HIV infection and clinically-normal ocular surface health, this study identifies subclinical group differences in corneal immune cells (potentially indicative of a heightened, pro-inflammatory activation state in the peripheral cornea) and corneal endothelial cell morphology that parallel those in chronic inflammatory disease. This study demonstrates the utility of Fun-IVCM to evaluate subclinical immune cell features in systemic disease, which could inform the future identification of biomarkers in immune-related conditions.

Keywords: immune cell, cornea, in vivo confocal microscopy, human immunodeficiency virus, immunology

Human immunodeficiency virus (HIV) impairs the adaptive immune system by infecting and progressively depleting $CD4^+$ T cells, leading to immunodeficiency and increased susceptibility to opportunistic infections. Lifelong antiretroviral therapy (ART), which suppresses viral replication and controls the viral load, has increased the lifespan of people with HIV.[1] Globally, the number of people with HIV aged >50 years increased from 5.7 million in 2016 to 7.5 million in 2020.[2] However, despite achieving near-equivalent life expectancy as the general population,[3] a sustained, low-grade inflammation and immune-activated state has been proposed to contribute to comorbidities and accelerate immunosenescence[4] in an increasingly older population living with HIV.

The transparency and accessibility of the human cornea allows in vivo confocal microscopy (IVCM) to reveal the sensory nerve supply and cellular components of both its innate and adaptive immune systems.[5–9] Myeloid cells are considered to predominate under homeostatic conditions, comprising epithelial dendritic cells (DCs) and stromal macrophages. Lymphocytes, recently identified as T cells, also patrol the corneal epithelium.[10] Our recently established method to track single immune cells—functional IVCM (Fun-IVCM)—enables characterization of dynamic cell

behaviors and how they are altered in non-homeostatic conditions.[7] Here, we leverage Fun-IVCM to compare the density, morphology, and dynamics of corneal DCs, T cells, and macrophages in older adults receiving ART for HIV infection with age-similar, healthy controls. An older adult population was specifically chosen for the study, as we expected that this age group would provide the greatest capacity to detect inter-group differences in subclinical indicators of corneal immune status. Anatomical features of the corneal epithelial nerves and endothelium were also quantified, alongside tear cytokine levels, to evaluate for signs of an accelerated-aging or a pro-inflammatory status. These novel analyses provide a comprehensive microstructural window into altered features of corneal sensory nerves, immune cell subsets, and a quiescent cellular layer in older adults with well-managed HIV infection and clinically normal ocular health.

Methods

Participants

This study was conducted in accordance with the Declaration of Helsinki in the Department of Optometry and Vision Sciences, The University of Melbourne (Victoria, Australia). Ethical approval was obtained from the Alfred Health Human Research Ethics Committee (ID no. 191-17). All participants provided written informed consent. As an exploratory study with no predefined hypothesis about potential intergroup differences, we recruited a convenience sample of HIV-diagnosed patients from the Melbourne Sexual Health Centre, Alfred Health (Victoria, Australia), approximately matched in age and sex distribution to a non-HIV control group. Control participants were recruited from advertisements on community noticeboards and mailing lists (e.g., University of the Third Age) and a database of previous research participants.

Participant inclusion criteria were: aged 60–80 years inclusive, best-corrected visual acuity ≥6/9.5 (20/32), absence of ocular health abnormality (confirmed by slit lamp biomicroscopy and non-mydriatic retinal fundus examination), no systemic conditions (aside from HIV in this participant group) or medications known to affect vision or ocular surface health (e.g., diabetes, allergic eye disease, autoimmune conditions), and English proficiency to complete the study surveys. Individuals with clinical evidence of prior corneal disease and/or self-reported prior corneal infection were excluded from participating.

Questionnaires and Clinical Examinations

Participant demographic and health information were obtained by interview and/or medical record review. Participants completed the Heaviness of Smoking Index questionnaire[8] if they self-reported current smoking. This tool (score range 0–6) categorizes nicotine dependence as low (score: 0–1), medium (2–4) or high (5–6). Participants completed the Ocular Surface Disease Index questionnaire[9] to quantify dry eye symptomatology (score range 0–100; score <13, no symptoms; 13–22, mild; 23–32, moderate; ≥33, severe). Clinical tests were conducted bilaterally to assess ocular surface health, in the following order: tear osmolarity (TearLab, Tear Corporation); grading of anterior blepharitis, meibomian gland dysfunction, temporal bulbar conjunctival redness, nasal bulbar conjunctival redness and limbal redness (Efron scale);[10] grading of nuclear, cortical and posterior subcapsular lens opacities (LOCS III scale);[11] fluorescein tear break-up time (average of three measures, after instilling one drop of sodium fluorescein); grading of corneal fluorescein staining, and temporal and nasal conjunctival lissamine green staining (Oxford scale);[12] upper and lower eyelid eversion for papillary conjunctivitis (Efron scale)[10]; and lid wiper epitheliopathy (Korb scale, horizontal length, and sagittal width staining for both eyelids).[13] All grading scales were applied using integer increments.

Corneal Imaging

Corneal IVCM imaging was performed with topical anesthesia (0.4% oxybuprocaine hydrochloride) on participants' right eyes using the Heidelberg Retinal Tomograph-III with Rostock Corneal Module, following our published protocols.[7,14] For static IVCM, the sequence-scan mode was used to capture non-overlapping images (400 × 400 µm area) of the central corneal basal epithelium (n = 12 areas) and endothelium (n = 4 areas). The sequence-scan mode acquires 100 frames at a nominally fixed plane of focus. For Fun-IVCM, five repeated sequence-scan and volume-scan (z-stack) images were captured of the basal epithelium and anterior stroma, at the whorl and ~2 mm inferior (peripheral) to the whorl, at 5.0 ± 1.5-minute intervals for up to 30 minutes. The corneal epithelial whorl provides a reproducible anatomical landmark for Fun-IVCM.[15]

Corneal Cell Characterization

Custom MATLAB (Version R2023a; The MathWorks, Natick, MA, USA) software[15] was used to create time-lapsed videos of the whorl and peripheral cornea, for the epithelium and stroma. Individual sequence-scans (100-frame videos) were first co-registered and dewarped to mitigate distortion resulting from eye motion during the scans. From each registered scan, a high-quality average image was generated to represent the tissue at a given time point. Time-lapsed image stacks were then generated by combining five time-separated, averaged images of the same tissue region at a consistent depth. Co-registration between the averaged images was conducted to maximize the stability of static background tissue, facilitating visualization of cell motility.[15] For the epithelium, nerve axons were used as static landmarks to register the image set; keratocytes were used for the stroma. Immune cells (DCs, T cells, macrophages) were identified based on their characteristic morphometry and motility.[7] Static and dynamic cell attributes (Table 1) were quantified by manual tracing and tracking, respectively, by a single observer in Image J.[16]

Corneal Nerve and Endothelial Cell Analysis

Epithelial nerve parameters were quantified for each participant by averaging data obtained from 12 non-overlapping images of the central cornea. ACCMetrics (University of Manchester, Manchester, UK)[17] was used to automatically delineate the nerve fibers and derive a suite of attributes (Table 1). Two to four non-overlapping images encompassing a tissue area >40,000 µm^2 were manually chosen for endothelial cell analysis;[18] individual cells were manually traced in Image J[16] and characterized using standard metrics (Table 1). Morphological parameters were quantified at cellular level and then averaged for each participant.

Table 1. Corneal Immune Cell and Nerve Parameters Quantified in This Study

Parameter	Cellular Elements Analyzed	Definition or Derivation
Cell morphology		
Cell area (μm^2)	DC, macrophage, endothelial cell	Area within the freehand tracing around the cell border
Cell perimeter (μm)		Total length of the freehand tracing around the cell border
Feret's diameter (μm)		The longest distance between two points on the cell border
Roundness (unitless, range 0–1)		A measure of how close the cell is to a perfect circle. Calculated by 4*area/(π*major_axis^2)
Solidity (unitless, range 0–1)		A measurement of how compact the cell is. Calculated by cell area/convex hull area
Field area (μm^2)	DC, macrophage	Area of the convex hull of the cell
Dendrite number	DC	The number of dendrite tips per cell
Cell dynamics		
dSEARCH index (μm/min)	DC	Cumulative distance of dendrite extension and retraction of all dendrite tips, from a single cell, divided by time, calculated for each time interval
Probing speed (μm/min)		Total distance of dendrite extension and retraction of each dendrite tip divided by total time, averaged for all dendrite tips from a single cell, over the total observation period
Mean instantaneous speed (μm/min)	T cell	Averaged instantaneous speeds, calculated by the track length between two consecutive time-points divided by time
Displacement speed (μm/min)		Net cell displacement divided by total time
Meandering index (range 0–1)		Net cell displacement divided by total cell track length (also known as confinement ratio)
Motility (motile or immotile)		An 'immotile' T cell was defined as a cell with a mean instantaneous speed <2 μm/min across all time intervals
Dancing index (%/min)	Macrophage	Calculated as a percentage, derived from calculating the nonoverlapped cell area divided by the total (summed) area, after colocalizing the same macrophage cell across two consecutive time intervals (based on aligning the centroids of the two cell shapes), normalized to time, and then averaged across all time intervals for a given macrophage
Nerve parameters[*]		
Corneal nerve fiber density [CNFD] (fibers/mm^2)	Epithelial (sub-basal) nerve plexus	Number of main nerve fibers in a given area of the cornea
Corneal nerve branch density [CNBD] (branches/mm^2)		Number of main nerve branches in a given area of the cornea
Corneal nerve fiber length [CNFL] (mm/mm^2)		Total length of all nerve fibers in a given area of the cornea
Corneal nerve total branch density [CTBD] (total branches/mm^2)		Total number of nerve branches in a given area of the cornea
Corneal nerve fiber area [CNFA] (mm^2/mm^2)		Total surface area occupied by all nerve fibers in a given region of the cornea
Corneal nerve fiber width [CNFW] (mm/mm^2)		Average width of the nerve fibers in a given area of the cornea
Corneal nerve fractal dimension [CNFrD] (unitless)		A measure of the complexity of the nerve pattern in a given area of the cornea

A description or derivation is included for each parameter to characterize corneal immune and endothelial cell morphology, immune cell dynamics, and sensory nerve anatomical features, for each cellular element analyzed.

DC, dendritic cell; dSEARCH, dendrite surveillance extension and retraction cycling habitude.

[*] ACCMetrics[17] standard nerve parameters.

Investigative Ophthalmology & Visual Science

Tear Collection and Protein Analyses

Before drop or dye instillation to the eye, non-stimulated (basal) tear samples (~10 µL/eye) were collected by microcapillary flow from the interior tear meniscus[19,20] and stored at −80°C. Cytokine levels were quantified using bead-based multiplex immunoassay (Immune Monitoring 65-Plex Human ProcartaPlex Panel; Thermo Fisher Scientific, USA) according to manufacturer instructions, using 3 µL of tear diluted in 22 µL of assay buffer. Samples were processed in the same analytical run (on a single plate) on a Luminex FlexMAP 3D (Luminex, TX, USA). Cytokine concentrations were interpolated using ThermoFisher ProcartaPlex software. Total tear protein and secretory immunoglobulin A (sIgA) were quantified using NanoDrop (Thermo Fisher Scientific, Waltham, MA, USA) and an in-house enzyme-linked immunosorbent assay,[20] respectively.

Statistical Analysis

Between-group, "per participant" data were compared using *t* tests (parametric data, Kolmogorov-Smirnov test), Mann-Whitney rank-sum tests (non-parametric data), or chi-squared tests for proportions, as appropriate, using Prism (version 10.3.1; GraphPad Software, San Diego, CA, USA). Analyses for immune cell densities ("per participant") and for immune cell morphology and dynamics ("per cell") were conducted by fitting linear mixed-effects models with restricted maximum likelihood (parametric data) or generalized linear mixed-effects models (non-parametric data). A random effect was incorporated to accommodate any potential within-participant correlation among cells. When an interaction was detected in the model, post hoc pairwise tests were performed with Tukey adjustment for multiple comparisons using R software with lme4 package (Version 4.3.0).[21] A P value <0.05 was considered statistically significant.

Results

Participant Characteristics

Table 2 summarizes participant demographic and clinical data. Age and sex were similar between groups. There were more current smokers in the HIV group ($P = 0.04$), ranging from low ($n = 1$), medium ($n = 2$), to high ($n = 1$) nicotine dependence, compared to none in the control group. On average, HIV participants had been diagnosed for 18 years and had been on their current ART for at least four years. All participants had either undetectable (<20 copies/mL, 14 of 16 participants) or non-viremic (<200 copies/mL) viral load, indicating effective ART. There were no between-group differences for any clinical ocular surface parameters or the degree of lens opacity (Supplementary Table S1).

Corneal Intraepithelial T Cells

In total, 617 corneal T cells ($n = 376$ control; $n = 241$ HIV, Fig. 1A) were analyzed across all participants. For T-cell density, there was no effect of group or corneal region (Fig. 1B). For cell motility, the group × region interaction was significant; with a greater proportion of motile cells in the HIV group (Fig. 1C, $P < 0.001$) and higher mean instantaneous (Fig. 1D, $P = 0.001$) and displacement cell speeds (Fig. 1E, $P < 0.001$) in the peripheral cornea relative to the whorl. At the whorl, HIV participants showed a higher proportion of T cells exhibiting arrested behaviors (Fig. 1C, $P = 0.008$), with lower speeds compared to controls (Fig. 1D, $P = 0.01$). An overall effect of corneal region was identified for the T cell meandering index, which was higher (indicative of more linear cell movement) in the periphery than the whorl (Fig. 1F, $P = 0.001$). Representative videos showing T-cell motility in HIV and control participants are provided in the Supplementary Material (Videos S1 and S2, respectively).

Corneal Intraepithelial Dendritic Cells

In total, 119 DCs ($n = 59$ control; $n = 60$ HIV) were analyzed across all participants (Fig. 2A). Although cell density was similar between groups, more DCs were observed in the peripheral cornea relative to the whorl (Fig. 2B, $P < 0.001$). In the HIV group, peripheral DCs were larger ($P < 0.001$) and rounder ($P = 0.04$) than in the whorl (Figs. 2C, 2D). For field area, an effect of region (whorl vs. peripheral, $P = 0.03$) but not group was observed (Fig. 2E).

Table 2. Participant Demographic and Clinical Characteristics

	Control ($n = 15$)	HIV ($n = 16$)	P Value
Demographics			
Age (years)	71 ± 5	67 ± 6	0.06*
Sex			0.96†
Male	14	15	
Female	1	1	
Current smokers			0.04†
Yes	0	4	
No	15	12	
HIV clinical characteristics			
Duration of HIV infection (months)	—	214 ± 116	—
$CD4^+$ T cell count at diagnosis (cells/mm^3)	—	432 ± 177	—
Most recent $CD4^+$ T cell count (cells/mm^3)	—	596 [512, 840]	—
Nadir $CD4^+$ T cell count after treatment (cells/mm^3)	—	290 ± 128	—
HIV viral load at diagnosis (RNA copies/mL)	—	45,947 ± 49,909	—
Duration of undetectable HIV viral load (months)	—	166 ± 87	—

HIV, human immunodeficiency virus; RNA, Ribonucleic acid.
Data are shown as either mean ± standard deviation, or median [interquartile range], as appropriate to the statistical analysis.
*P value from independent t-tests between groups.
†P value from χ^2 test of proportions between groups.

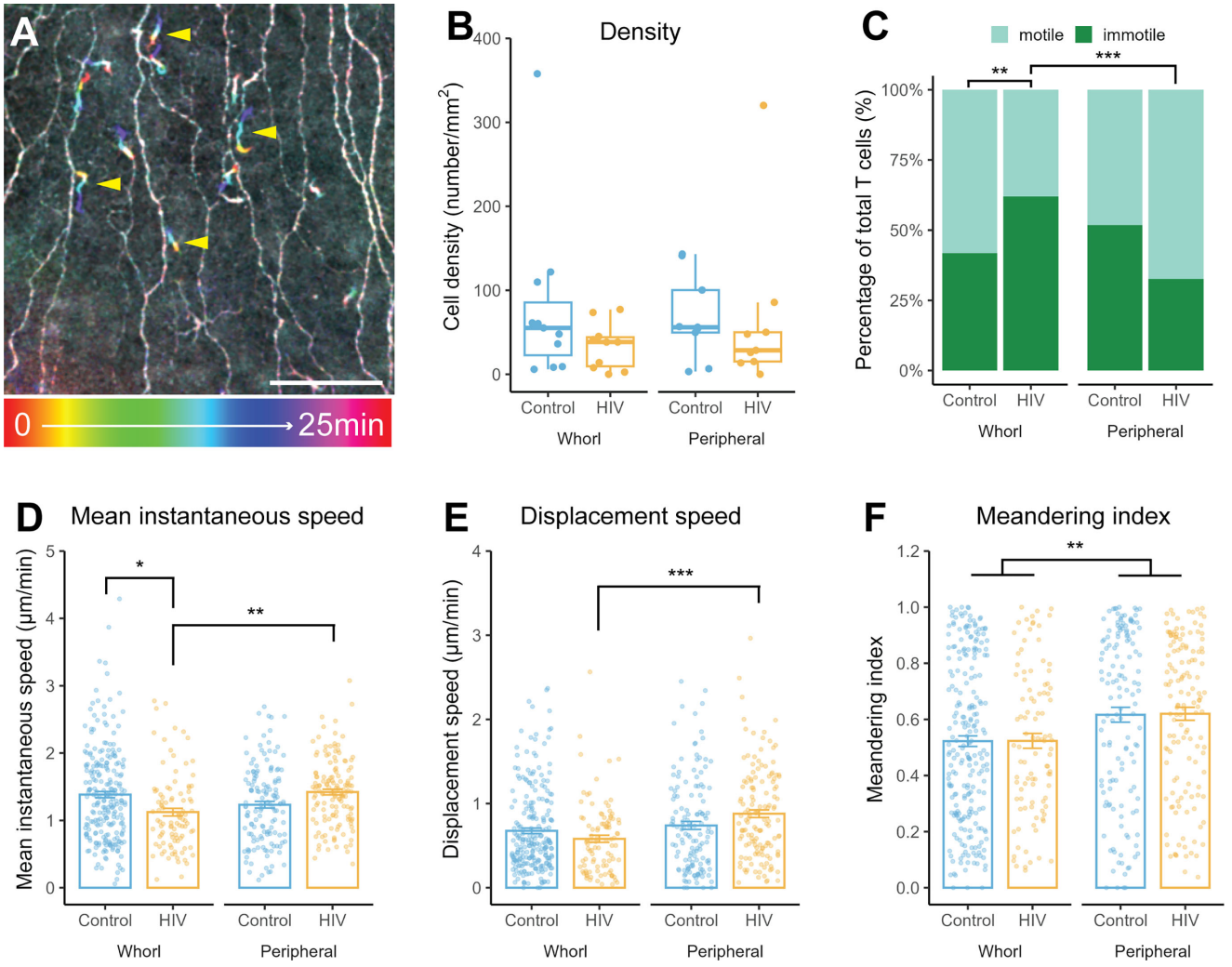

Figure 1. Dynamic features of corneal intraepithelial T-cells in the control and HIV participant groups. **(A)** A representative color projection image of a Fun-IVCM time-lapsed video, over 25 minutes, showing intraepithelial T-cells (*arrowheads*) in the peripheral cornea. *Scale bar*: 100 µm. **(B)** T-cell density was similar between the study groups, across both corneal regions; data are shown as median and interquartile range. **(C)** At the corneal whorl, the proportion of motile T-cells (i.e., cells with a mean instantaneous speed > 2 µm/min over at least one time interval) was relatively higher in controls. Within the HIV group, the proportion of motile T-cells was higher in the peripheral cornea than the whorl. **(D)** T-cell mean instantaneous speed was relatively higher in controls than HIV participants at the corneal whorl and, within the HIV group, cell mean instantaneous speed was higher in the peripheral than whorl region. **(E)** T-cell displacement speed was higher in the peripheral cornea, relative to the whorl, in the HIV group only. **(F)** An overall effect of region, but not group, was evident for the meandering index, being relatively higher in the peripheral cornea. Unless otherwise stated, data are shown as mean ± SE, with individual data points, at the per cell level, as symbols. Linear mixed-effects models were used for all analyses. If an interaction was detected, pairwise tests were performed with Tukey adjustment **(C, D,** and **E)**. *$P < 0.05$, **$P < 0.01$, ***$P < 0.001$. Non-significant comparisons are not shown.

There were no between-group or region-dependent differences for the number of dendrite tips (Fig. 2F) or the dynamic attributes of dSEARCH index and probing speed (Figs. 2F–H).

Corneal Anterior Stromal Macrophages

In total, 96 stromal macrophages (n = 44 control; n = 52 HIV) were analyzed across all participants (Supplementary Fig. S1A). There were no between-group or between-region differences for cell density (Supplementary Fig. S1B), morphology (Supplementary Figs. S1C, S1D) or dancing index (Supplementary Fig. S1E). Overall, macrophages at the whorl had higher mean instantaneous speeds than those in the periphery (Supplementary Fig. S1F, $P = 0.003$).

Corneal Sensory Nerves

For central corneal epithelial nerves (Supplementary Fig. S2), all quantitative parameters were similar between groups, aside from a relatively greater nerve fiber width in the HIV group (Supplementary Fig. S2D, $P = 0.004$).

Corneal Endothelium

Central corneal endothelial cell density (Fig. 3B) was similar between groups, whereas cell area ($P = 0.02$), perimeter ($P = 0.03$) and Feret's diameter ($P = 0.03$) were larger in the HIV compared to control group (Figs. 3C–E). There were no between-group differences for cell roundness or solidity.

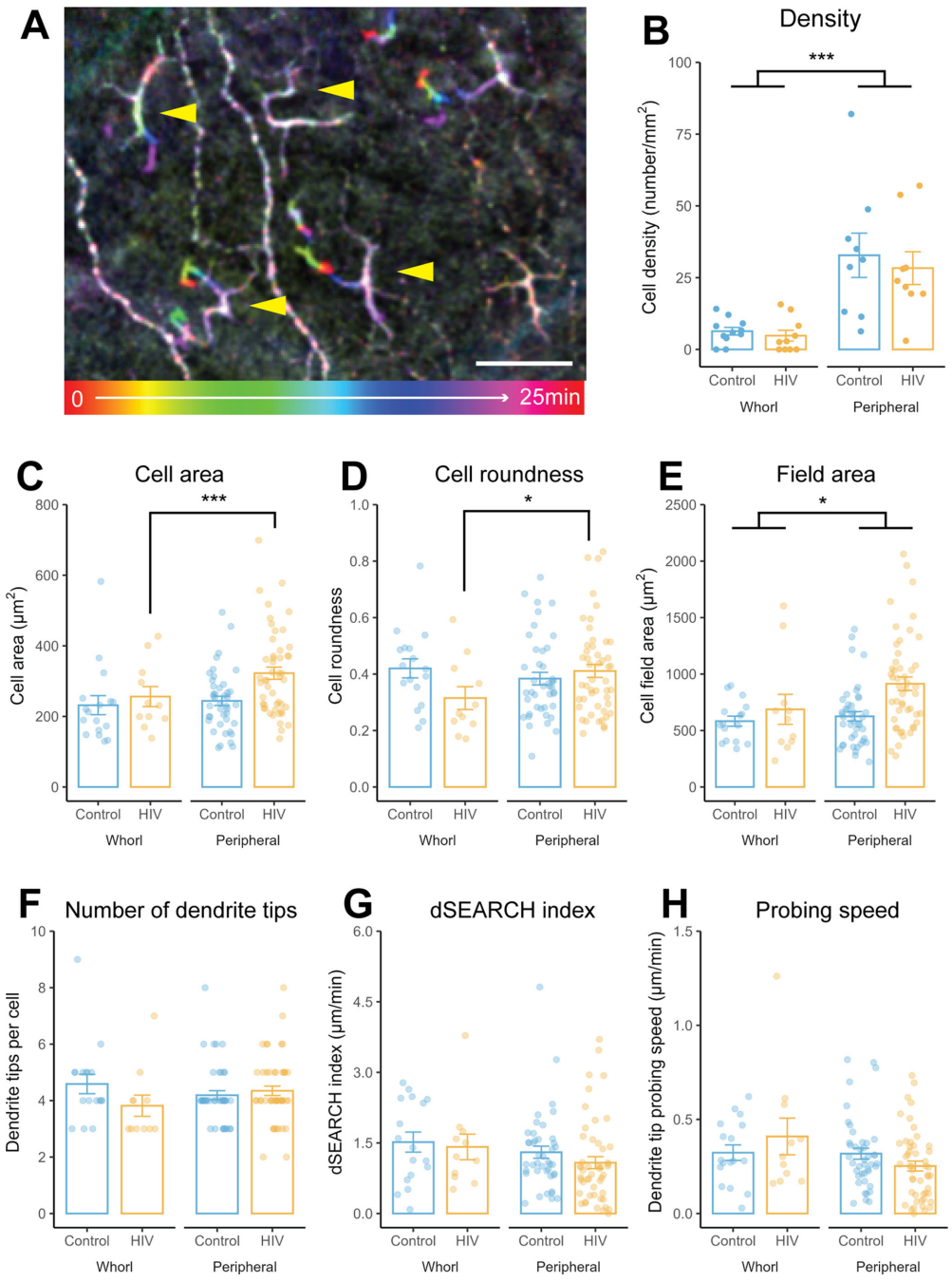

Figure 2. Morphodynamic features of corneal intraepithelial dendritic cells (DCs) in the control and HIV participant groups. **(A)** A representative color projection image of a Fun-IVCM time-lapsed video, over 25 minutes, showing intraepithelial DCs (*arrowheads*) in the peripheral cornea. *Scale bar*: 50 µm. **(B)** Overall, DC density was higher in the peripheral cornea, relative to the corneal whorl, but no between-group difference was observed. **(C)** In the HIV group only, DC cell areas were larger in the peripheral cornea relative to the whorl. **(D)** In the HIV group only, DCs were rounder in the peripheral cornea relative to the whorl. **(E)** For DC field area, an effect of region (whorl vs. peripheral) but not participant group was observed. There were no inter-group or inter-region differences for the **(F)** number of dendrite tips, **(G)** dSEARCH index or **(H)** probing speed. Data are shown as mean ± SE, with individual data points, at the per cell level, as symbols. Linear mixed-effects models were used for all analyses. If an interaction was detected, pairwise tests were performed with Tukey adjustment **(C, D)**. $^{*}P < 0.05$, $^{***}P < 0.001$. Nonsignificant comparisons are not shown.

Tear Proteins

No between-group differences were observed for tear total protein and sIgA (Supplementary Table S1) or tear cytokine levels (Supplementary Table S2).

Discussion

This study investigated whether the in vivo morphodynamic features of corneal immune cell subsets differ between a cohort of HIV-positive individuals receiving effective ART

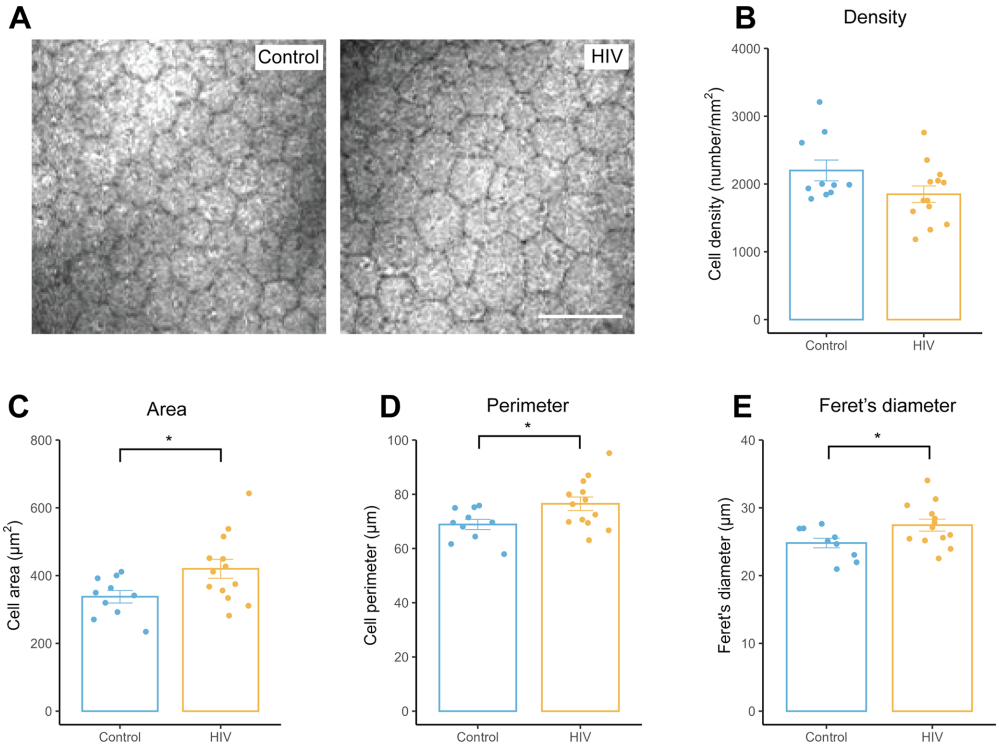

Figure 3. Corneal endothelial cell features in the control and HIV participant groups. **(A)** Representative static IVCM images showing corneal endothelial cells in each group. *Scale bar*: 50 µm applies to both images. **(B)** Cell density was similar between the groups. **(C)** Cell area, **(D)** perimeter and **(E)** Feret's diameter were higher in the HIV group relative to the control group. Data are shown as mean ± SE, with individual data points, at the per participant level, as symbols. Student's *t*-tests were performed for all analyses. $^*P < 0.05$. Non-significant comparisons are not shown.

and a healthy age-matched control group. By quantifying nerve morphology, endothelial cell parameters, and tear cytokine levels, we also evaluated whether older individuals with well-controlled HIV showed signs of accelerated ocular surface aging or inflammation. All HIV-positive participants had $CD4^+$ T cell counts within normative ranges (500–1500 cells/mm^3)[22] and viral load levels of <200 copies/mL.[23] Participant groups had similar ocular surface parameters, indicative of clinically normal anterior eye health. This finding aligns with prior research by our group for anterior ocular surface and tear cytokine parameters between HIV-positive and -negative participants, apart from greater meibomian gland dropout that correlated with HIV disease severity.[20] In the present study, the main between-group differences were subclinical, defined by relatively thicker central corneal nerve fibers, differences in the in vivo dynamics of corneal T cells and morphology of DCs, and a larger corneal endothelial cell size, in the ART-treated HIV-positive group.

Prior cross-sectional studies have reported lower corneal nerve fiber density, length and branch density, and higher tortuosity in individuals with HIV relative to healthy controls.[24,25] In the current study, across both participant groups, absolute values for these corneal nerve attributes were relatively low compared to those reported previously in younger cohorts, likely reflecting an older demographic and general manifestation of physiological age-related changes to corneal nerves.[26] A relatively higher central corneal nerve fiber width (CNFW) was found in the HIV-positive group. Wider corneal nerves have been documented in multiple ocular states, including dry eye disease[27], blepharoptosis[28] and neuropathic corneal pain.[29] Greater CNFW may reflect a loss of small nerve fibers, which has been observed in non-human primates with simian immunodeficiency virus,[30] a closely related virus to HIV causing a similar disease profile, with relative preservation of the thicker nerve bundles that is characteristic of small fiber neuropathy.[31,32] Although beyond the scope of the present study, there is increasing interest in HIV-related neuropathy, which may result from the neurotoxic effects of the virus and long-term ART.[33] The observed higher (thicker) CNFW in people with HIV may reflect early neurodegenerative changes consistent with small fiber neuropathy, or alternatively, axonal swelling secondary to local neuroinflammation.[34–36] Prior animal studies have suggested that chronic immune activation and $CD4^+$ T cell responses contribute to corneal nerve damage, independent of corneal epitheliopathy.[37,38] These data raise the possibility that local neuroimmune interactions may be involved in corneal neuropathic changes. Future longitudinal studies could consider whether CNFW is an early indicator of small fiber neuropathy in people with HIV, given that corneal imaging is a more accessible (non-invasive) approach than techniques such as peripheral nerve skin biopsies.

To date, the potential impact of HIV (or its treatment) on immune cell motility has not been studied in vivo in clinical populations because of the technical inability to track individual immune cells in living human tissues. Using multi-photon intravital microscopy, T-cell dynamics were quantified in the lymph nodes of humanized mice, with HIV-infected $CD4^+$ T cells showing reduced motility relative to uninfected cells.[39] A major outcome of the present study is

identification of region-dependent differences in the motility of human corneal epithelial T cells in older people living with HIV. Consistent with the reported impairment of T-cell motility in experimental animal models,[39] we found lower T-cell speeds in the whorl region of HIV corneas relative to controls. However, this effect was not apparent in the peripheral cornea, where epithelial T cells had significantly higher motility relative to the (paracentral) whorl in the HIV group. The differences in cell dynamics were observed in the absence of statistically significant between-group differences in T cell density, despite the known effect of HIV infection in systemically depleting $CD4^+$ T cells. That said, we did observe a trend toward lower T-cell density in the HIV-positive, relative to the healthy control, group ($P = 0.095$). We acknowledge the study may not be sufficiently powered to detect a difference in this outcome. Lower corneal T-cell speeds, which might feasibly exist in other organs, could reflect altered immune cell surveillance or migratory capacity that is not captured by a clinically-derived total T-cell count. With no detectable differences in tear cytokines, the observed differences in cell motility might not be due to inflammatory mediators but could reflect cell-intrinsic changes. For example, the relative abundance of $CD4^+/CD8^+$ T cells may differ, manifesting as an overall different distribution in cell speeds. Further research is required to interpret the functional significance of the observed T-cell mobility differences.

We have previously shown that in states of increased ocular immune activation (e.g., seasonal allergy, contact lens wear), human corneal epithelial T cells show higher in vivo motility.[7] This difference in cell dynamics appears characteristic of pro-inflammatory tissue environments,[40] and may indicate increased adaptive immune surveillance. The observed eccentricity-dependent asymmetry in T-cell dynamics within HIV-positive corneas, whereby the peripheral region shows a greater patrolling cell profile, may reflect its proximity to the vascularized limbal and conjunctival tissues and a relative prioritization of immune surveillance in this region.[41,42]

Similar region-dependent differences were evident for corneal epithelial DC morphology in the HIV-positive group, defined by larger and rounder cells in the periphery relative to the whorl, without differences in dynamic behaviors. In general, increased DC size is associated with a shift from an immature to mature activation state.[43] DC maturation induces a spectrum of metabolic, cellular, and gene transcription alterations that optimize antigen presentation to T cells. In human corneas, larger DC sizes have been associated with pro-inflammatory states that include allergic conjunctivitis,[44] dry eye disease,[44] and diabetes mellitus.[45] Together, these findings suggest that the peripheral cornea of HIV-infected individuals may show a heightened immune state, defined by more active T cells and larger DCs. Further research is required to determine the functional and clinical significance of these findings.

The endothelium represents another potentially informative corneal cellular layer. Comprising a monolayer of cells, corneal endothelial cells are post-mitotic and undergo a progressive decline in density with age, at an average rate of ~0.6% per year.[46,47] In the present study, corneal endothelial cell density was similar between the age-matched groups, per previous reports,[48,49] but distinct morphological differences were observed. We found that endothelial cells in the HIV-positive group had a larger field area, perimeter, and Feret's diameter; such differences likely result from cell enlargement and spreading, which are considered compensatory adaptations to maintain tissue function.[50] Similar morphological alterations to the corneal endothelial cell mosaic have been described in systemic inflammatory diseases, including chronic kidney disease,[51] gout[52] and active Graves' ophthalmopathy.[53]

We acknowledge some considerations when interpreting the data, including multiple comparisons with an exploratory approach and the potential to have measured other complementary aspects of ocular surface status (e.g., central corneal thickness) and peripheral nerve health (e.g., neuropathy assessments). The presented data provide rationale for future studies investigating these attributes to further define how HIV infection and associated ART might affect aging and inflammatory status. Such future research would optimally include the additional quantification of systemic (blood) inflammatory markers and peripheral nerve status (such as via biopsy), to map to the relevant corneal imaging findings.

In conclusion, this study uniquely describes the in vivo morphodynamic features of corneal immune cells in older adults with well-controlled HIV infection relative to a comparator group of age-matched controls. Distinct corneal immune cell features were evident in the HIV-positive cohort, involving eccentricity-dependent differences in epithelial T cell motility and DC morphology. In addition, the HIV-positive group had relatively thicker central corneal nerve fibers and larger endothelial cells, which may reflect subclinical differences that align with the presence of relatively pro-aging and pro-inflammatory profiles.

Acknowledgments

Supported by an Australian Research Council Discovery Project Grant (DP230102105) to L.E.D., S.N.M., and H.R.C., an Early Career Researcher grant to B.N.N. from The University of Melbourne, and an R.M. Gibson grant to B.N.N. from the Australian Association of Gerontology. The funding organizations had no role in the design and conduct of the study; collection, management, analysis, and interpretation of the data; preparation, review, or approval of the manuscript; and decision to support the manuscript for publication.

Disclosure: **S. Karunaratne**, None; **M. Wu**, AU2023901150 (P); **X. Yu**, None; **S.J. Kent**, None; **J. Silvers**, None; **P. Bedggood**, AU2023901150 (P); **A. Metha**, AU2023901150 (P); **S.N. Mueller**, AU2023901150 (P); **K.J. Selva**, None; **A.W. Chung**, None; **H.R. Chinnery**, AU2023901150 (P); **B.N. Nguyen**, None; **L.E. Downie**, AU2023901150 (P)

References

1. Antiretroviral Therapy Cohort Collaboration. Life expectancy of individuals on combination antiretroviral therapy in high-income countries: a collaborative analysis of 14 cohort studies. *Lancet*. 2008;372:293–299.
2. Autenrieth CS, Beck EJ, Stelzle D, Mallouris C, Mahy M, Ghys P. Global and regional trends of people living with HIV aged 50 and over: Estimates and projections for 2000–2020. *PLoS One*. 2018;13:e0207005.
3. Marcus JL, Leyden WA, Alexeeff SE, et al. Comparison of Overall and Comorbidity-Free Life Expectancy Between Insured Adults With and Without HIV Infection, 2000–2016. *JAMA Netw Open*. 2020;3:e207954.
4. Sieg SF, Shive CL, Panigrahi S, Freeman ML. Probing the Interface of HIV and Inflammaging. *Curr HIV/AIDS Rep*. 2021;18:198–210.

5. Galletti JG, de Paiva CS. The ocular surface immune system through the eyes of aging. *Ocul Surf*. 2021;20:139–162.
6. Wu M, Hill LJ, Downie LE, Chinnery HR. Neuroimmune crosstalk in the cornea: The role of immune cells in corneal nerve maintenance during homeostasis and inflammation. *Prog Retin Eye Res*. 2022;91:101105.
7. Downie LE, Zhang X, Wu M, et al. Redefining the human corneal immune compartment using dynamic intravital imaging. *Proc Natl Acad Sci USA*. 2023;120: e2217795120.
8. Heatherton TF, Kozlowski LT, Frecker RC, Rickert W, Robinson J. Measuring the heaviness of smoking: using self-reported time to the first cigarette of the day and number of cigarettes smoked per day. *Br J Addict*. 1989;84:791–800.
9. Schiffman RM, Christianson MD, Jacobsen G, Hirsch JD, Reis BL. Reliability and validity of the Ocular Surface Disease Index. *Arch Ophthalmol*. 2000;118:615–621.
10. Efron N. Grading scales for contact lens complications. *Ophthalmic Physiol Opt*. 1998;18:182–186.
11. Chylack LT, Jr., Wolfe JK, Singer DM, et al. The Lens Opacities Classification System III. The Longitudinal Study of Cataract Study Group. *Arch Ophthalmol*. 1993;111:831–836.
12. Bron AJ, Evans VE, Smith JA. Grading of corneal and conjunctival staining in the context of other dry eye tests. *Cornea*. 2003;22:640–650.
13. Korb DR, Herman JP, Greiner JV, et al. Lid wiper epitheliopathy and dry eye symptoms. *Eye Contact Lens*. 2005;31:2–8.
14. Wu M, Zhang X, Karunaratne S, et al. Intravital imaging of the human cornea reveals the differential effects of season on innate and adaptive immune cell morphodynamics. *Ophthalmology*. 2024;131:1185–1195.
15. Bedggood P, Wu M, Zhang X, et al. Improved tracking of corneal immune cell dynamics using in vivo confocal microscopy. *Biomed Opt Express*. 2024;15:6277–6298.
16. Rasband WS. *ImageJ, U. S. National Institutes of Health*, Bethesda, Maryland, USA. Available at: https://imagej.net/ij/download.html. Accessed July 01, 2023.
17. Petropoulos IN, Alam U, Fadavi H, et al. Rapid automated diagnosis of diabetic peripheral neuropathy with in vivo corneal confocal microscopy. *Invest Ophthalmol Vis Sci*. 2014;55:2071–2078.
18. Kheirkhah A, Saboo US, Marmalidou A, Dana R. Overestimation of corneal endothelial cell density in smaller frame sizes in in vivo confocal microscopy. *Cornea*. 2016;35:363–369.
19. Jackson DC, Zeng W, Wong CY, et al. Tear Interferon-gamma as a biomarker for evaporative dry eye disease. *Invest Ophthalmol Vis Sci*. 2016;57:4824–4830.
20. Nguyen BN, Chung AW, Lopez E, et al. Meibomian gland dropout is associated with immunodeficiency at HIV diagnosis: implications for dry eye disease. *Ocul Surf*. 2020;18:206–213.
21. R Core Team. *R: A language and environment for statistical computing*. Vienna: R Foundation for Statistical Computing. 2021.
22. Garcia SAB, Guzman N. Acquired immune deficiency syndrome CD4+ count. *StatPearls*. Treasure Island, FL: StatPearls Publishing; 2023.
23. U.S. Department of Health and Human Services. *Plasma HIV-1 RNA (Viral Load) and CD4 Count Monitoring*. ASHM; 2023.
24. Petropoulos IN, Al-Mohammedi A, Chen X, et al. The utility of corneal nerve fractal dimension analysis in peripheral neuropathies of different etiology. *Transl Vis Sci Technol*. 2020;9:43–43.
25. Kemp HI, Petropoulos IN, Rice ASC, et al. Use of corneal confocal microscopy to evaluate small nerve fibers in patients with human immunodeficiency virus. *JAMA Ophthalmol*. 2017;135:795–800.
26. Chin JY, Liu C, Lee IXY, et al. Impact of age on the characteristics of corneal nerves and corneal epithelial cells in healthy adults. *Cornea*. 2024;43:409–418.
27. Giannaccare G, Pellegrini M, Sebastiani S, Moscardelli F, Versura P, Campos EC. In vivo confocal microscopy morphometric analysis of corneal subbasal nerve plexus in dry eye disease using newly developed fully automated system. *Graefes Arch Clin Exp Ophthalmol*. 2019;257:583–589.
28. Zhang Z, Lu S, Jiang Y, Sun S. Assessing the corneal sub-basal nerve plexus by in vivo confocal microscopy in patients with blepharoptosis. *Ann Med*. 2022;54:227–234.
29. Liu C, Lin MT, Lee IXY, et al. Neuropathic corneal pain: tear proteomic and neuromediator profiles, imaging features, and clinical manifestations. *Am J Ophthalmol*. 2024;265:6–20.
30. Dorsey JL, Mangus LM, Oakley JD, et al. Loss of corneal sensory nerve fibers in SIV-infected macaques: an alternate approach to investigate HIV-induced PNS damage. *Am J Pathol*. 2014;184:1652–1659.
31. Themistocleous AC, Ramirez JD, Serra J, Bennett DL. The clinical approach to small fiber neuropathy and painful channelopathy. *Pract Neurol*. 2014;14:368–379.
32. Jazebi N, Evans C, Kadaru HS, et al. HIV-related neuropathy: pathophysiology, treatment and challenges. *J Neurol Exp Neurosci*. 2021;7:15–24.
33. Lu HJ, Fu YY, Wei QQ, Zhang ZJ. Neuroinflammation in HIV-related neuropathic pain. *Front Pharmacol*. 2021;12:653852.
34. Deeks SG, Tracy R, Douek DC. Systemic effects of inflammation on health during chronic HIV infection. *Immunity*. 2013;39:633–645.
35. Nasi M, Pinti M, Mussini C, Cossarizza A. Persistent inflammation in HIV infection: established concepts, new perspectives. *Immunol Lett*. 2014;161:184–188.
36. Ishizaka A, Koga M, Mizutani T, et al. Unique gut microbiome in HIV patients on antiretroviral therapy (ART) suggests association with chronic inflammation. *Microbiology Spectrum*. 2021;9(1):10–1128.
37. Vereertbrugghen A, Pizzano M, Cernutto A, et al. CD4(+) T cells drive corneal nerve damage but not epitheliopathy in an acute aqueous-deficient dry eye model. *Proc Natl Acad Sci USA*. 2024;121:e2407648121.
38. Vereertbrugghen A, Pizzano M, Sabbione F, et al. An ocular Th1 immune response promotes corneal nerve damage independently of the development of corneal epitheliopathy. *J Neuroinflammation*. 2023;20:120.
39. Murooka TT, Deruaz M, Marangoni F, et al. HIV-infected T cells are migratory vehicles for viral dissemination. *Nature*. 2012;490:283–287.
40. Teijeira A, Hunter MC, Russo E, et al. T cell migration from inflamed skin to draining lymph nodes requires intralymphatic crawling supported by ICAM-1/LFA-1 Interactions. *Cell Rep*. 2017;18:857–865.
41. Liu J, Li Z. Resident innate immune cells in the cornea. *Front Immunol*. 2021;12:620284.
42. Akpek EK, Gottsch JD. Immune defense at the ocular surface. *Eye*. 2003;17:949–956.
43. Chinnery HR, Zhang XY, Wu CY, Downie LE. Corneal immune cell morphometry as an indicator of local and systemic pathology: a review. *Clin Exp Ophthalmol*. 2021;49:729–740.
44. Tajbakhsh Z, Golebiowski B, Stapleton F, et al. Increased dendritic cell density and altered morphology in allergic conjunctivitis. *Eye*. 2023;37:2896–2904.
45. Lagali NS, Badian RA, Liu X, et al. Dendritic cell maturation in the corneal epithelium with onset of type 2 diabetes is

Investigative Ophthalmology & Visual Science

associated with tumor necrosis factor receptor superfamily member 9. *Sci Rep*. 2018;8:14248.
46. Wang Q, Dou S, Zhang B, et al. Heterogeneity of human corneal endothelium implicates lncRNA NEAT1 in Fuchs endothelial corneal dystrophy. *Mol Ther Nucleic Acids*. 2022;27:880–893.
47. Thomasy SM, Leonard BC, Greiner MA, Skeie JM, Raghunathan VK. Squishy matters—corneal mechanobiology in health and disease. *Prog Retin Eye Res*. 2024;99:101234.
48. Cetin EN, Kutlu SS, Parca O, Kutlu M, Pekel G. Corneal and anterior chamber morphology in human immunodeficiency virus-1-infected patients without opportunistic infections. *Eye Contact Lens*. 2018;44 Suppl 2:S281–s284.
49. Pathai S, Lawn SD, Shiels PG, et al. Corneal endothelial cells provide evidence of accelerated cellular senescence associated with HIV infection: a case-control study. *PLoS One*. 2013;8:e57422.
50. Lee J, Jung E, Heur M. Injury induces endothelial to mesenchymal transition in the mouse corneal endothelium in vivo via FGF2. *Mol Vis*. 2019;25:22–34.
51. Kanawa S, Jain K, Sagar V, Yadav DK. Evaluation of changes in corneal endothelium in chronic kidney disease. *Indian J Ophthalmol*. 2021;69:1080–1083.
52. Kösekahya P, Üçgül Atılgan C, Atılgan KG, et al. Corneal endothelial morphology and thickness changes in patients with gout. *Turk J Ophthalmol*. 2019;49:178–182.
53. Zhou M, Wu D, Yu F, et al. Corneal endothelium: a promising quantitative index for graves ophthalmopathy activity evaluation. *Am J Ophthalmol*. 2021;230:216–223.

Investigative Ophthalmology & Visual Science